

# X-ray spectroscopy of the active dM stars: AD Leo and EV Lac

S. Sciortino<sup>1</sup>, A. Maggio<sup>1</sup>, F. Favata<sup>2</sup>, and S. Orlando<sup>3</sup>

<sup>1</sup> Osservatorio Astronomico di Palermo, Piazza del Parlamento 1, I-90134 Palermo, Italy

<sup>2</sup> Astrophysics Division – Space Science Department of ESA, ESTEC, Postbus 299, 2200 AG Noordwijk, The Netherlands

<sup>3</sup> Solar System Division – Space Science Department of ESA, ESTEC, Postbus 299, 2200 AG Noordwijk, The Netherlands

Received 3 August 1998 / Accepted 21 October 1998

**Abstract.** We present results of an analysis of new observations of the active M dwarfs AD Leo (GJ 388) and EV Lac (GJ 873), performed with the X-ray satellite SAX, and compare them with both published and new analyses of ROSAT PSPC observations of these stars. The PSPC spectra can be fitted with one- (EV Lac) or two-component (AD Leo) isothermal MEKAL models, and very low metallicity ( $\sim 0.1$  solar); we have found clear evidence of spectral variations in correspondence of a large flare observed during one of the PSPC observations of EV Lac, requiring the addition of a second component with  $\log T \sim 7.5$  to fit the flare spectrum. The SAX light-curves of AD Leo and EV Lac also show the occurrence of several flares. A two-component model does not provide an adequate fit of the SAX spectra, regardless of the value of coronal metallicity. These spectra require at least three thermal MEKAL components and best-fit coronal plasma metallicity below solar for AD Leo and only marginally below solar for EV Lac, with 90% confidence ranges on  $Z/Z_{\odot} = 0.22$ -0.35 and 0.36-1.11, respectively.

We have also fitted the SAX spectra of AD Leo and EV Lac with model spectra from constant cross-section static coronal loops. One-loop models fail to fit the observed spectra. A second loop component, that accounts for most of the plasma emission at high energy, is required to obtain a fit of statistical quality just slightly worse than the 3-T fits. In the case of EV Lac both the 2-loop and the 3-T fits are unable to reproduce the observed emission below 0.5 keV. The available evidence points toward the existence of various (at least two) main classes of coronal emitting structures: the dominant one is composed of hundreds of compact loops, with relatively low maximum temperature and length smaller than 0.1 the stellar radius, covering no more than 1% of stellar surface; the second class, responsible for the high energy emission, is composed at least of tens of quite elongated loops, covering a very small fraction of stellar surface. We find no-evidence of loops with length comparable to the stellar radius.

**Key words:** X-rays: stars – stars: late-type – stars: activity – stars: abundances – stars: individual: AD Leo – stars: individual: EV Lac

## 1. Introduction

The first extensive efforts to model and fit X-ray spectra of stellar coronal sources date back to the era of the *Einstein* satellite (Schmitt et al. 1990). The low spectral resolution ( $\Delta E/E \sim 1$ ), and bandpass (0.16–4.5 keV) of the *Einstein* IPC, allowed to perform X-ray spectral analyses only with simple models, having just few free parameters (cf. Vaiana 1983, Schmitt et al. 1990). IPC data showed that the X-ray spectra of solar-type stars, observed with sufficient photon statistics, usually require models including two emission components from an optically thin plasma (Raymond & Smith 1977). In the case of dMe stars the fits usually result in one component at few million degrees, and a second one at few tens of million degrees. While the need of two thermal components does not necessarily imply the existence of two distinct emitting “regions” at different temperatures in the stellar coronae, it certainly reflects the presence of a (complex) thermal structure in stellar coronae. In fact, equally good fits to the IPC spectra have been also obtained using a continuous emission measure (EM) model (Schmitt et al. 1990), and the analysis of the broad-band EXOSAT data (Pallavicini et al. 1988) has shown the presence of multi-temperature plasma.

This description has been confirmed and extended by the analysis of spectra gathered with the Position Sensitive Proportional Counter (PSPC) on board ROSAT, thanks to its improved spectral resolution and larger sensitivity. Model spectra with at least two components are required in most cases to provide acceptable fits, such as for low X-ray luminosity giants (Maggio et al. 1994), or old-disk and halo population dM stars (Micela et al. 1997), but more complex models, such as power-law emission measure distributions (Preibisch 1997) or detailed coronal loop model spectra (Maggio & Peres 1997, Ventura et al. 1998) result in comparable quality fits while providing a deeper insight on the structure of stellar coronae.

The recent analysis of ASCA, EUVE and SAX spectra (White 1996; Drake 1996; Favata 1998; Pallavicini 1998 and references therein cited) of several nearby and/or active solar-type stars has further reinforced a description of stellar coronal spectra in terms of scaled version of the solar emission. Moreover the improved spectral resolution of the ASCA and EUVE observations has opened the, still debated, issue of anomalous abundances in stellar coronae, affected either by the so-called

**Table 1.** Characteristics of program stars

Star	Sp. Type	Kin. Pop.	D <sup>a</sup> (pc)	R <sub>*</sub> /R <sub>⊙</sub> <sup>b</sup>	M/M <sub>⊙</sub> <sup>b</sup>	log g <sup>b</sup>	v sin(i) <sup>c</sup> (km/sec)	B <sup>d</sup> (kG)	f <sub>B</sub> %
AD Leo (GL 388)	M4.5 Ve	YD	6.15	0.41	0.34	4.73	6.2±0.8	3.8	73
EV Lac (GL 873)	M4.5 Ve	YD	5.08	0.41	0.34	4.73	6.9±0.8	5.2	90

<sup>a</sup> Parallaxes from the Hipparcos Catalogue (ESA SP-1200, 1997) available also at <http://cdsweb.u-strasbg.fr/Cats.html>.

<sup>b</sup> We report the value of stellar radius, mass and gravity we have adopted for computing the coronal loop models.

<sup>c</sup> From Delfosse et al. (1998)

<sup>d</sup> Magnetic field strength and surface filling factor from Saar (1990)

Metal Abundance Deficiency syndrome stars (see Drake 1996 for a review about this issue), or by the occurrence of the so-called FIP effect, observed in the solar corona (Meyer 1985). This issue has been recently investigated in the light of the new stellar data (Favata 1998; Pallavicini 1998) taken with the SAX X-ray astronomy satellite (Boella et al. 1997a).

However it is worth to stress that: i) coronal abundances can be considered “anomalous” only if different from measured photospheric abundances; any abundance different from the canonical solar one cannot be considered “per se” as an anomaly; ii) derived coronal abundances need to be well constrained and reliable; extensive simulations are required to gain confidence on coronal abundances derived from X-ray spectral fits of medium resolution spectra (Favata et al. 1997, Favata et al. 1998). These latter studies clearly show that the issue of individual element abundances, if pursued with CCD-like X-ray spectra, requires high statistical quality spectra, usually with more than  $5 \cdot 10^4$  counts, while the determination of overall coronal metallicity can be pursued even with spectra with only  $10^4$  counts.

There are several reasons that makes the study of the coronal emission of the dMe stars a worth effort. First of all, their X-ray emission level – either expressed in terms of X-ray luminosity,  $L_X$ , or in terms of the X-ray luminosity scaled to the bolometric luminosity,  $L_X/L_{Bol}$  – makes them the most intense coronal emitters, with the only exceptions of the so-called active binaries, and of pre-main-sequence stars, hence they are a good test-bed for any proposed mechanism for the heating of stellar coronae. Their internal structure, reflected by their cool photospheres, should minimize any contribution by non-magnetic (acoustic) heating processes making easier to pin point the characteristic features of the coronal magnetic heating mechanism and their relation to any kind of dynamo activity, either based on a scaled version of the solar  $\alpha - \omega$  dynamo or on the more elusive turbulent dynamo (cf. Durney et al. 1993) that has been suggested to be at work in the (almost) fully convective late dM stars (Stern et al. 1995). Another important issue is that of the transient activity, down to the “microflare” level, as important contributor to the heating of dM coronae and the relation between this (micro)flaring activity and any dynamo action at work in the interior of these stars. Finally it is worth to mention that dM stars are by far the more numerous of the coronal sources in our (and likely any other) Galaxy, so that a better knowledge of their coronal spectra is important for any improvement in our

capability to accurately predict the stellar contribution to the diffuse X-ray background.

As a step to gain further insight in the above questions we have obtained observations of the active dMe stars AD Leo and EV Lac with the SAX X-ray astronomy satellite as part of the AO-1 Core Program.

AD Leo (GJ 388) is a single dM4.5e star at a trigonometric distance of 6.15 pc, EV Lac is a single dM4.5e star at a trigonometric distance of 5.08 pc. They are both well known flare stars, extensively studied over an ample range of wavelengths and are known to emit from infrared up to X-rays. Their space velocities make them members of young disk population based on the criterion of Eggen (1973). They are among the few M stars for which, adopting the Zeeman broadening technique, it has been possible to derive the (mean) value of the surface magnetic field in the spots, with the associated area coverage (Saar 1990). It is noteworthy that the deduced magnetic fields for AD Leo and EV Lac are of the order of  $10^3$  Gauss (similar to the intensity of magnetic field in solar spots) with area coverage fraction above 70% (i.e. well above the typical spot coverage in the Sun). This is a clear evidence that some kind of dynamo action should be at work in these almost fully convective stars.

These two stars are the two strongest dMe coronal emitters with X-ray fluxes to the Earth  $f_X \sim 3 \cdot 10^{-11}$  erg sec<sup>-1</sup> cm<sup>-2</sup> for AD Leo (Barbera et al. 1993; Schmitt et al. 1995) and  $f_X \sim 4 \cdot 10^{-11}$  erg sec<sup>-1</sup> cm<sup>-2</sup> for EV Lac (Schmitt et al. 1995), as measured with the *Einstein* and ROSAT observatories. Relevant information on AD Leo and EV Lac are summarized in Table 1.

The IPC spectrum of AD Leo cannot be adequately fitted, for an assumed solar composition of emitting plasma, either with 1-T or 2-T Raymond-Smith plasma emission models, or with a continuous power-law emission measure distribution (Schmitt et al. 1990).

After the early *Einstein* observation, better quality PSPC and ASCA spectra have been gathered (see below for details on PSPC data analysis). Two ASCA observations have been performed: the first, publicly available at the time of this work, was obtained during the PV phase, but unfortunately the adopted observing strategy prevents any reliable analysis of the accumulated spectrum; the second, being more recent, was not publicly available at the time of this work.

EV Lac was not observed with the *Einstein* observatory, but it has been extensively studied with the PSPC on-board ROSAT (see below for results of the analysis of the archive

**Table 2.** Summary of available PSPC data

Star	ROR	Obs. Start UT	Exp. Time (sec)	Offaxis (arcmin)	Net Collected Counts (0.2–2.4 keV)
AD Leo	200076	08 MAY 1991 06:12:00	26520	0.0	62808
EV Lac	200984	13 JUL 1992 13:04:07	2675	0.7	28810
EV Lac	201583	08 JUL 1993 22:00:50	3337	41.0	5076
EV Lac	201584	09 JUL 1993 21:57:19	3753	41.0	5408
EV Lac	201585	10 JUL 1993 21:48:02	4563	41.2	4923
EV Lac	201586	11 JUL 1993 21:19:37	5934	41.6	7103
EV Lac	201587	12 JUL 1993 21:07:56	7535	41.1	8854

PSPC spectra). No ASCA observation of EV Lac was performed at the time of this work.

In this paper we present the results of the analysis of the new SAX data, acquired with the Low Energy Concentrator Spectrometer (LECS, Parmar et al. 1997), which covers the energy range 0.1–10 keV with a spectral resolution  $\Delta E/E \simeq 20\%$  at 1 keV and scaling as  $E^{-1/2}$ , and with the Medium Energy Concentrator Spectrometers (MECS's, Boella et al. 1997b), which cover the energy range 1.5–10 keV with a spectral resolution  $\Delta E/E \simeq 8\%$  at 6 keV and scaling as  $E^{-1/2}$ ; we also compare our findings with the published and newly obtained results from the analysis of the archive PSPC data.

The accumulated SAX spectra, with a resolution better than that of the *Einstein* IPC and the ROSAT PSPC, allow us to constrain the characteristics of coronal spectra of AD Leo and EV Lac both in terms of simple multi-temperature plasma models and in terms of self-consistent magnetic loop models.

The spectral fits and light curves of PSPC data are discussed in Sect. 2. We present our new SAX data and their temporal and simple multi-temperature spectral analyses in Sect. 3. In Sect. 4 we present our modeling of the SAX spectra based on loop atmospheres, self-consistently computed with variable coronal metal abundance, and discuss our principal findings.

## 2. The PSPC observations of AD Leo and EV Lac

There is one single PSPC observation of AD Leo whose characteristics are summarized in Table 2.

EV Lac has been observed six times with the ROSAT PSPC; a list of available PSPC observations and related information is summarized in Table 2. In five cases (8–12 July 1993) the observations have been taken purposely at large off-axis angle for smearing out the effect of the PSPC entrance window support grid in order to study time variability of EV Lac (below few hundreds seconds) without the spurious modulation introduced by the partial source shadowing due to satellite 400 second oscillations (wobbling).

PSPC spectra and light-curves extraction has been performed using PROS V2.4. The entire spectral analysis, including the analysis of SAX spectra of Sect. 3, has been performed using the XSPEC V.10 package and the so-called MEKAL plasma emissivity model and adopting simple multi-component thermal plasma models.

### 2.1. AD Leo PSPC spectrum

The accumulated spectrum was already modeled (Giampapa et al. 1996, hereafter G96) with two distinct temperature components from a thermal plasma in ionization equilibrium, whose emission is described by the Raymond-Smith emissivity model (Raymond & Smith 1977, Raymond 1988). In order to obtain a statistically acceptable fit, e.g. a fit that results in a  $\chi^2$  probability higher than 3%<sup>1</sup>, the coronal metallicity,  $Z$ , needs to be lower than the solar one. We report in Table 3 the 90% confidence limit (for a single interesting parameter) on the fit parameters, obtained by Giampapa et al. (1996). In order to make easy and more consistent the comparison with the results of the rest of our analysis, based on a different plasma emissivity code, we have re-analyzed the AD Leo PSPC spectrum. Our results are also reported in Table 3. It is worth to note that: a) it is impossible to obtain a statistically acceptable two-component fit if we keep fixed the value of hydrogen column density to  $N_H = 10^{18} \text{ cm}^{-2}$ , that is within a factor two from the value recently derived by the analysis of a EUVE spectroscopic observation of AD Leo (cf. Cully et al. 1997); b) our analysis based on the MEKAL plasma emissivity model results in higher temperatures and in much greater  $EM_L/EM_H$  ratio than the published ones (cf. G96) derived adopting the Raymond-Smith plasma emissivity code. It is worth noting that the individual emission measure  $EM_L$  and  $EM_H$  obtained with our fit are both significantly lower than those reported by G96 because the MEKAL plasma emissivity per unit emission measure is greater than the one predicted by the Raymond-Smith model.

### 2.2. EV Lac PSPC spectra

Since analysis of the EV Lac PSPC spectra has not been published yet, we have analyzed the available data retrieved from the public archive.

Before proceeding with the spectral analysis we have constructed the PSPC light-curves of the available data. For the ROR's from 201583 to 201587 spanning 5 consecutive days, we have constructed a single light curve, while we have separately considered the light curve from ROR 200984 taken one

<sup>1</sup> We have adopted 3% since this is a typical value below which fit statistic is mainly driven by systematic uncertainties in calibration

**Table 3.** Best fit of PSPC spectra

Star	Metallicity ( $Z/Z_{\odot}$ )	$N_H$ ( $10^{19} \text{ cm}^{-2}$ )	$\log(T_L)$ (K)	$EM_L$ ( $10^{51} \text{ cm}^{-3}$ )	$\log(T_H)$ (K)	$EM_H$ ( $10^{51} \text{ cm}^{-3}$ )	Prob. (%)	$f_X$ ( $10^{-11} \text{ erg/s/cm}^2$ ) [0.1–2.4 keV]
AD Leo	0.10	1.7	6.82	16.0	7.22	2.7	8.2	3.13
(G96)	[0.10–0.11] [0.07–0.13]	[1.4–2.1] [2.1–3.3]	[6.72–6.85] [7.44–7.74]	[15.3–17.2] <sup>a</sup> [10.2–17.6]	[7.06–7.73] <sup>a</sup> [7.99–8.06]	[1.8–3.4] [19.6–27.4]		
EV Lac (200984)	0.13	1.0	6.89	18.4	7.56	10.6	27.0	8.10
(200984–fl)	[0.10–0.15]	....	[6.85–6.92]	[13.4–23.4]	[> 7.29]	[8.1–14.6]		
(201583)	0.14	1.0	6.93	7.7	7.56	22.8	48.3	15.8
(201583)	[0.11–0.20]	...	[6.83–6.97]	[3.8–11.0]	[> 7.23]	[16.5–40.0]		
(201584)	0.078	1.0	6.93	6.6	....	...	94.8	1.60
(201584)	[0.068–0.088]	...	[6.90–6.97]	[6.4–6.8]	....	...		
(201584)	0.084	1.0	6.82	6.3	....	...	73.5	1.43
(201584)	[0.073–0.096]	...	[6.78–6.85]	[6.0–6.5]	....	...		
(201585)	0.087	1.0	6.72	4.9	...	...	53.	1.01
(201585)	[0.070–0.11]	....	[6.67–6.76]	[4.6–5.1]	...	...		
(201586)	0.065	1.0	6.77	5.6	...	...	99.	1.13
(201586)	[0.055–0.077]	....	[6.74–6.81]	[5.4–5.8]	...	...		
(201587)	0.06	1.0	6.83	5.4	...	...	14.2	1.15
(201587)	[0.057–0.072]	....	[6.80–6.86]	[5.2–5.5]	...	...		
Joint–2	0.078	1.0	6.88	6.4	...	...	39.8	1.50
Joint–2	[0.071–0.085]	...	[6.85–6.90]	[6.3–6.6]	...	...		
Joint–3	0.068	1.0	6.78	5.3	...	...	4.3	1.10
Joint–3	[0.063–0.075]	...	[6.76–6.81]	[5.2–5.4]	...	...		

The reported parameter uncertainty ranges are computed at 90% confidence level assuming a single interesting parameter.

<sup>a</sup> In order to compute those ranges we have kept fixed  $N_H$  and  $T_L$  to their best-fit values.

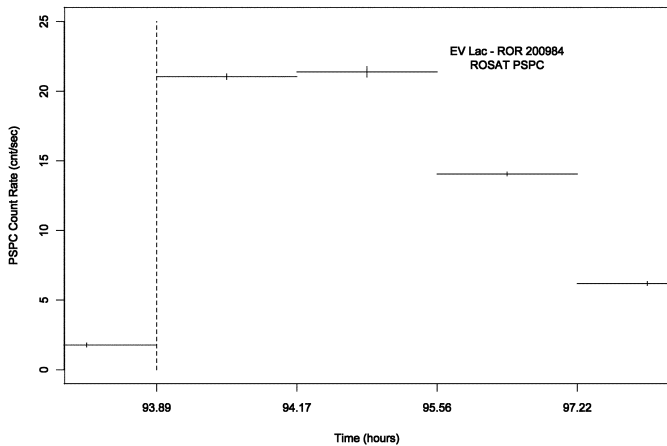


**Fig. 1.** PSPC light-curve of EV Lac, accumulated in 1000 sec time bins, for the ROR 200984. Times are referred to the first data point taken about 100 hours before the rest of the observation. The vertical dashed line marks the separation between the two observation segments. During the second part of the observation a very intense flare increases by about a factor 10 the coronal emission of EV Lac. The level of coronal emission outside the flare was similar to that observed one year later (cf. Fig. 2).

year before (and with a well different source off-axis angle). The resulting light curves are shown in Figs. 1 and 2.

All the PSPC spectra, with the only exception of the spectrum collected during an intense flare (ROR 200984, cf. Fig. 1), can be fitted with single-temperature emission model, but with global coronal metallicity much lower than solar. In performing all these fits, since EV Lac is quite nearby, we have fixed the amount of interstellar hydrogen column density  $N_H = 10^{19} \text{ cm}^{-2}$ . As a matter of fact if we leave  $N_H$  free to vary, the actual best-fit values are within a factor two of the chosen value.

In order to verify that the successful description of the collected spectra with a simple 1-T model is not dictated by the available number of hours of counts we have taken advantage of the relatively small time separation among the five observations from ROR 201583 to 201587 and have attempted to jointly fit these five PSPC spectra, but the fit was unsuccessful either with a 1-T or with a 2-T models, even with coronal metallicity left free to vary. As a further step in this analysis we have noted that these 5 PSPC spectra can be divided into 2 groups consisting of two (201583 and 201584, hereafter Joint-2) and three (201585, 201586, and 201587, hereafter Joint-3) PSPC spectra having similar “shapes” and have repeated the fit separately for the Joint-2 and the Joint-3 data sets. In both cases we have success-

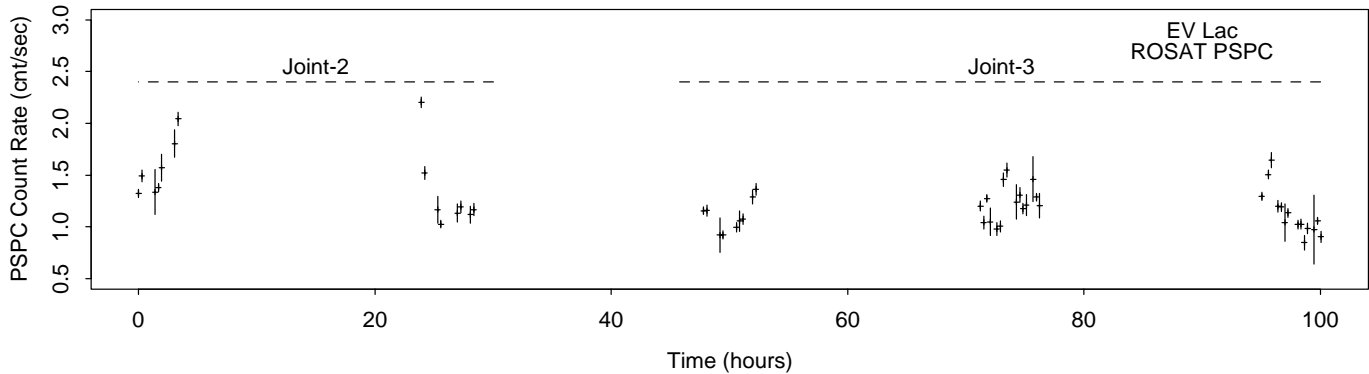


**Fig. 2.** PSPC light-curve of EV Lac, accumulated in 1000 sec bin size, obtained combining 5 distinct observations taken in 5 consecutive days. Notice that the data are suggestive of a coronal variability up to a factor 2 over the time scale explored. The horizontal dashed lines above the data points indicate the Joint-2 and the Joint-3 data we have analyzed.

fully fitted the available spectra with simple 1-T models having almost the same coronal metallicity but with the “Joint-2” set yielding somewhat higher temperature and emission measure than the “Joint-3” data set. This latter result has convinced us that the ability to fit the observed PSPC spectra with 1-T model is not driven by the counting statistics, but it likely reflects the actual shape of the EV Lac coronal emission measure distribution of which the PSPC is mainly sensible to the component(s) below  $\log T = 7.0$  unless higher temperature component are prominent like in the case of the flare (see below).

The single spectrum that cannot be described with a 1-T model and that was accumulated during an intense flare can instead be adequately fitted with a 2-T plasma emission model and coronal metallicity  $\sim 0.1$  solar. We have also fitted the spectrum collected just at the peak of the flare (indicated with the label 200984-fl in Table 3) in order to investigate possible variations of the best-fit model parameters. This latter fit yields essentially the same results of those obtained from the analysis of the entire observation.

The results of all our fits are summarized in Table 3 where we list both the best-fit values and the 90% confidence intervals computed considering a single “interesting” parameter. This table clearly shows that i) except for the strong flare, the PSPC spectra of EV Lac can be described by best fit 1-T models with derived parameters that are compatible within the error bars with a single value, ii) a coronal metallicity lower than solar ( $Z \sim 0.1$ ) is required to obtain good fits in all cases, iii) during the flare an high-temperature component has to be added to obtain a best fit, while the low-temperature component remains unchanged; iv) the limited spectral resolution and energy bandpass of the ROSAT PSPC, is unable to well constrain the value of the flare high-temperature component. This can be appreciated considering the contour plots shown in Fig. 3.

### 3. The SAX observations of AD Leo and EV Lac

The SAX observation of AD Leo was performed on April 23–34, 1997, and resulted in an effective exposure time of 43.3 ks for the three MECS units, and of 19.6 ks for the LECS.

The SAX observation of EV Lac was performed on December 7–8, 1997, and resulted in an effective exposure time of 33.9 ks for the two MECS<sup>2</sup>, and of 9.7 ks for the LECS.

The LECS exposure time is always significantly shorter than the MECS exposure time, because the LECS was operated during Earth dark time only, at the time of both observations.

The LECS data were reduced with the SAX-LEDAS V.1.4.0 pipeline software, while the MECS data were reduced using the SAXPIPE package. The default screening criteria defined in the processing software were applied, and inspection of the light curve for both the source and the local background showed that no additional screening was necessary.

The extraction of source counts to construct source spectra and light-curves was performed using the FTOOLS V4.0 package, adopting the interactive Xselect tool. The source extraction radius in the case of the LECS was 8.2 arcmin, corresponding to 35 instrumental pixels (95% encircled energy fraction at 1 keV), centered on the source centroid position. For the MECS we have adopted a source extraction radius of 4 arcmin, corresponding to 30 pixels in the detector coordinate system (about 95% encircled energy fraction over the bandpass). A visual examination of the LECS and the MECS images allows us to verify the stability of the aspect solution and to confirm that the adopted extraction regions are fully satisfactory.

The background spectrum was extracted from the LECS and the MECS’s standard background observations, obtained by adding up a set of long pointings of sky regions free of detectable sources. The response matrix for the LECS observations was computed using the current release (3.01) of the LEMAT software. Public available detector response matrices (known as “MECS{1,2,3}\_SEPT97”) were used for each of the available MECS’s.

The source spectra were re-binned so to have at least 30 counts per energy bin, and bins with energies below 0.1 and above 7.0 keV were discarded in the case of LECS, while for the MECS spectra we have retained the bins with energies between 1.5 and 7.0 keV.

<sup>2</sup> In the time separating the two observations one of the three MECS’s has developed an unrecoverable problem and has been turned off.

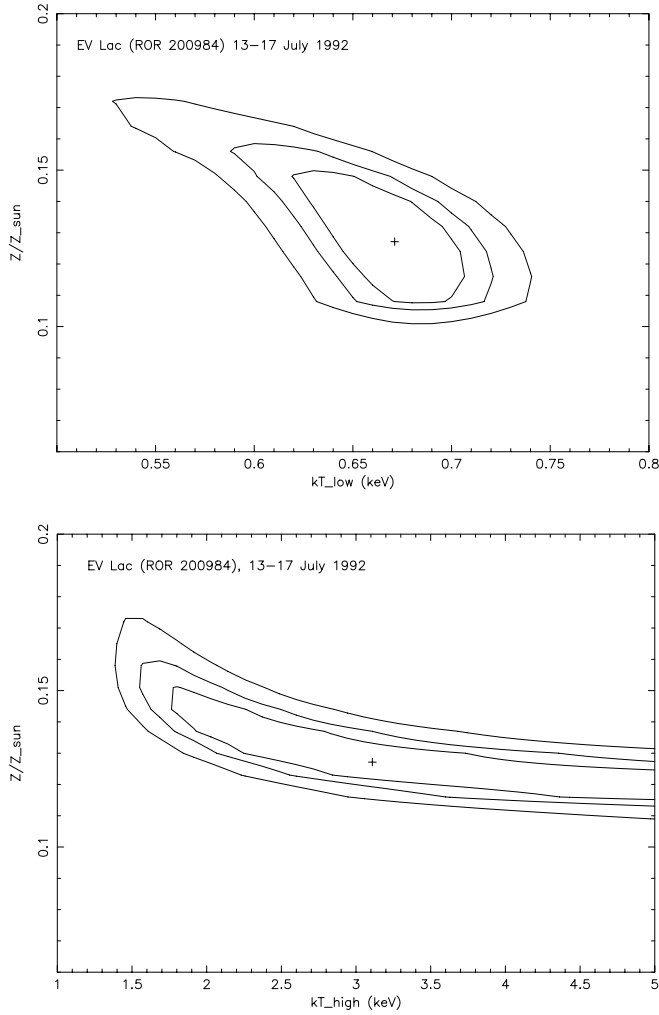


**Fig. 3.** **a** *upper-panel* Contour plot of the  $\chi^2$  in the  $kT_L$ , metallicity plane for the best-fit of the PSPC EV Lac spectrum taken during the strong flare. **b** *lower-panel* Contour plot of the  $\chi^2$  in the  $kT_H$ , metallicity plane for the best-fit of the same data set of panel **a**. The contours correspond to the 68, 90 and 99% confidence levels for the two interesting parameters (cf. Avni 1976, Lampton et al. 1976) in each panel. Note that with the available PSPC spectrum we cannot constrain the value of the high temperature.

The resulting (background-subtracted) source count rates and the estimated background rate for the source extraction region are summarized in Table 4.

### 3.1. The SAX X-ray light-curves

In order to increase the signal-to-noise ratio of the light-curves for these relatively weak SAX sources, we have taken advantage of the combined MECS's data and standard background observations produced by the SAX-SDC.

#### 3.1.1. AD Leo

The SAX observation of AD Leo spans approximately one day and allows us to follow its temporal behavior on time scales

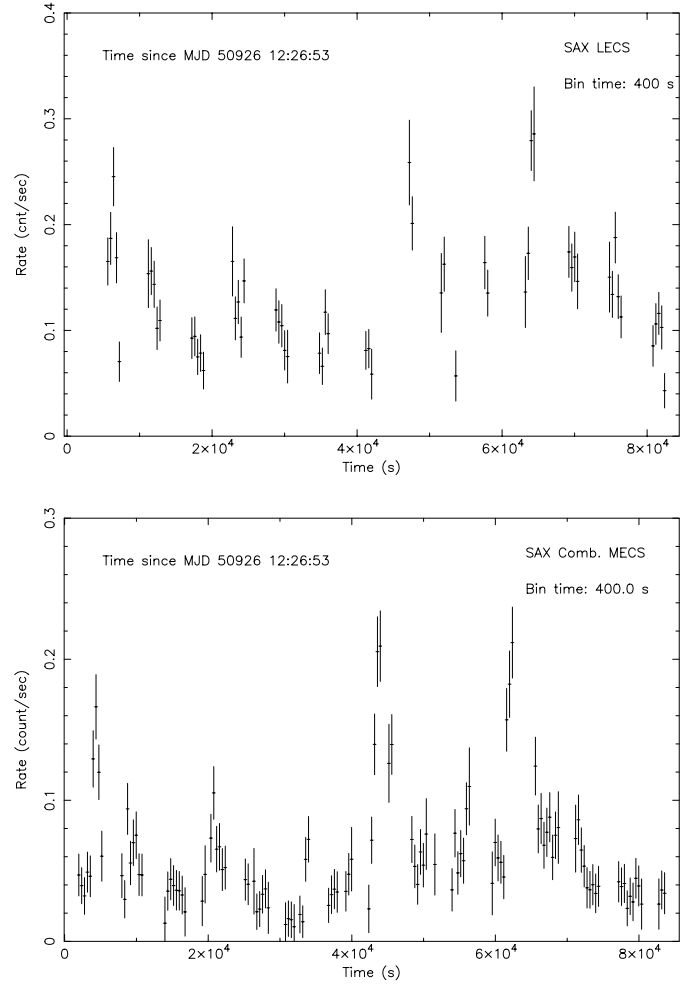


**Fig. 4.** **a** *upper-panel* The light curve of the SAX/LECS observation of AD Leo accumulated in 400 second bins, shows that the coronal emission level of this star is highly variable. **b** *lower-panel* The light curve of AD Leo accumulated in 400 sec bins, from the three combined MECS detectors onboard of SAX. The curve shows the occurrence of flares at about 6, 42, and 60 ks since the beginning of the one day long observation.

**Table 4.** Summary of count rates during the SAX observations

Star	Instrument	Source Rate (cnt/ks)	Background Rate (cnt/ks)
AD Leo	LECS	$126 \pm 2.5$	$20.2 \pm 0.82$
	MECS-1	$12.3 \pm 0.53$	$3.4 \pm 0.13$
	MECS-2	$22.0 \pm 0.71$	$2.9 \pm 0.12$
	MECS-3	$23.2 \pm 0.73$	$3.3 \pm 0.13$
EV Lac	LECS	$99.3 \pm 3.4$	$20.8 \pm 0.43$
	MECS-2	$24.3 \pm 0.9$	$2.9 \pm 0.12$
	MECS-3	$24.3 \pm 0.9$	$3.3 \pm 0.13$

from thousands of seconds up to one day. The resulting X-ray light curves, accumulated in 400 sec bins, for the LECS and the three combined MECS detectors are shown in Fig. 4.

Before proceeding with the analysis of the source light-curves we have analyzed the temporal behavior of the LECS and MECS image background applying the  $\chi^2$  and the Kolmogorov – Smirnov tests. Both tests indicate that the LECS and the MECS background are consistent with being constant, hence any observed variability is intrinsic to the source.

The LECS light curve (see Fig. 4) shows evidence of variability up to a factor 2 on a time scale of few thousands seconds, associated to the occurrence of flares (and possibly of other low-amplitude variability), such as those occurring at about 6, 45, and 62 ks since the beginning of the observation. A simple  $\chi^2$  test allows us to reject the null-hypothesis that the LECS emission comes from a constant source with high statistical confidence, a result confirmed also by the Kolmogorov – Smirnov test.

The MECS light-curve (Fig. 4) shows evidence for intense source variability. This is confirmed both by a simple  $\chi^2$  test and a Kolmogorov – Smirnov test. From the inspection of Fig. 4 it is evident the occurrence of, at least, 3 flares during the 1 day long observation, occurring at  $\sim 6$  ks (flare A), at  $\sim 45$  ks (flare B) and  $\sim 62$  ks (flare C) from the beginning of the observation. The peak count rates of these flares are  $\sim 4$ –5 times higher than the “quiescent” coronal emission level. Fitting a simple exponential decay model to data we have obtained decay times of 0.8 ks, 4.0 ks, and 4.4 ks for the flares A, B and C, respectively. These decay times are similar to that of compact solar flares, even if flare C seems to have a more complex temporal structure, with a slow rising time. The MECS light curve suggests the occurrence of less intense flares at other times, but the limited counting statistics prevent any further detailed analysis to verify their existence. However, the overall appearance of LECS and MECS light curves strongly indicates that a large fraction (30–50%) of the overall emitted X-rays occurs in flares.

### 3.1.2. EV Lac

As for AD Leo the SAX observation of EV Lac spans approximately one day. With the same procedure adopted for AD Leo we find that the LECS and combined MECS image backgrounds are consistent with being constant.

We show in Fig. 5 the background-subtracted LECS and combined MECS light-curves. Both curves suggest the presence of variability, whose existence has been confirmed by applying the  $\chi^2$  and the Kolmogorov-Smirnov tests. The MECS light curve shows two intense flares, occurring respectively 20 and 60 ks since the beginning of the observation, plus some less extreme variability. The decay times of the two flares derived with formal fits are about 4.5 ks and 1.4 ks, respectively.

### 3.2. Fit of SAX spectra

While it would be very interesting in view of source variability to perform time-resolved spectroscopy, this is prevented by the limited counting statistics of the source. In order to maximize the overall statistics of the fitting process we have jointly fitted the available LECS and MECS spectra. However, contrary to

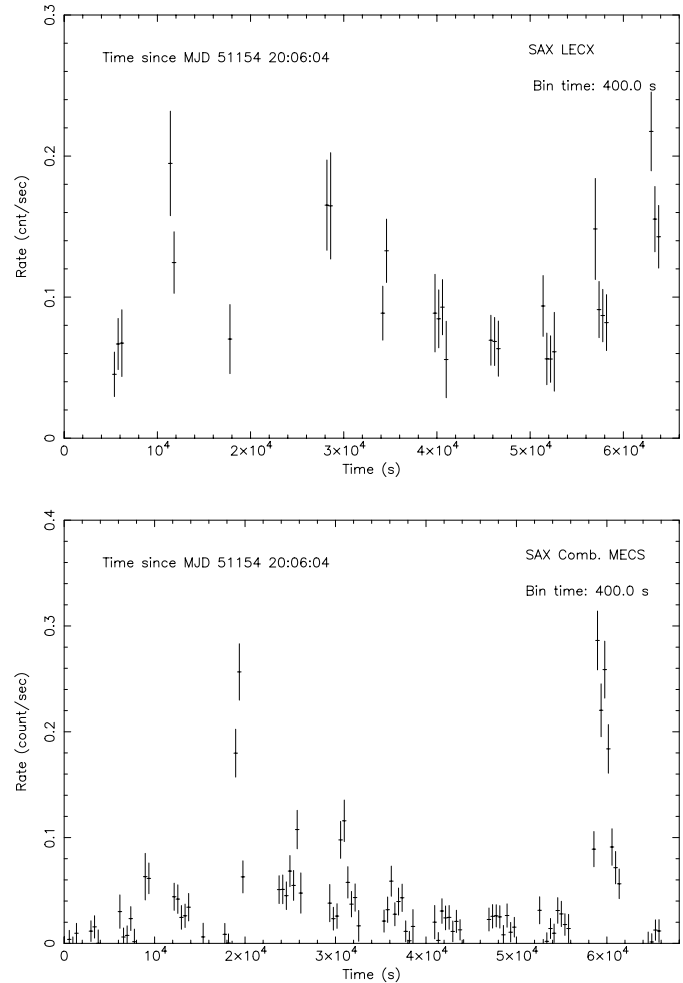


**Fig. 5.** **a** upper panel The light curve of the SAX/LECS observation of EV Lac accumulated 400 second bins, shows that the coronal emission level of this star is highly variable. **b** lower panel The light curve of EV Lac accumulated in 400 sec bins, from the combined two MECS detectors onboard of SAX. The curve shows the occurrence of flares at about 20, and 60 ks since the beginning of the one day long observation.

light-curve studies, we have preferred to treat each SAX MECS spectrum individually. In performing the fit we have assumed a constant normalization among the four detectors fixed in such a way that a source of given flux yields in the LECS 70% of the count-rate in any of the three MECS (that instead are all equivalent).

As demonstrated by an extensive set of simulations presented by Favata et al. (1997), LECS spectra allow us to get fair diagnostic capabilities for the global metallicity of coronal plasmas, thanks to the wide spectral coverage. The region below the carbon edge ( $E \simeq 0.3$  keV) is particularly important because typical coronal sources show a large photon flux in that region and a continuum emission with few and relatively weak lines, while the region around 1 keV is dominated by line emission from the Fe L complex. We take advantage of the wider band-pass of the LECS and MECS spectra to constrain both the global coronal metallicity and the thermal structure of the

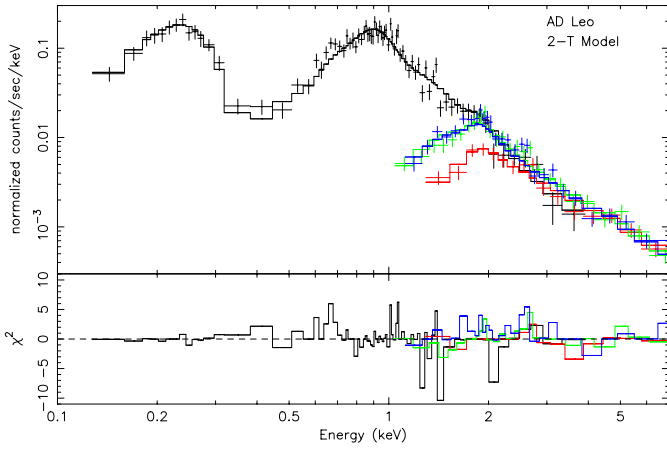


**Fig. 6.** The observed SAX spectra of AD Leo together with the best-fit two-temperature MEKAL spectrum, yielding a global metallicity 0.14 times solar. The bottom panel y-axis shows the (signed) contribution of each bin to the total  $\chi^2$ .

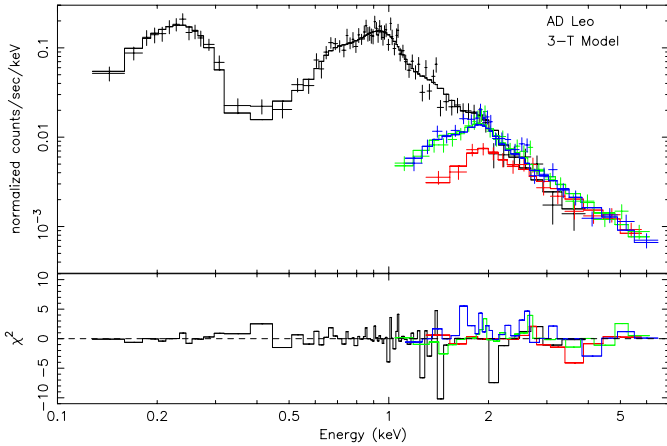


**Fig. 7.** The observed SAX spectra of AD Leo together with the best-fit three-temperature MEKAL spectrum, yielding a global metallicity 0.25 times solar. Note that most of improvement in the fit occurs in the spectral region around 0.6 keV. The bottom panel y-axis shows the (signed) contribution of each bin to the total  $\chi^2$ .

emitting plasma. The low statistics of the present SAX spectra, together with the spectral resolution above 0.6 keV lower than for the ASCA/SIS, makes unrealistic the analysis with variable individual abundances (as we will show in the following, acceptable fits can be found varying only the global metallicity in the fit).

### 3.2.1. The SAX spectra of AD Leo

Given the small source distance, the results of exploratory fits and the result obtained by Cully et al. (1997) we have decided to keep fixed the value of hydrogen column density to  $N_H = 10^{18} \text{ cm}^{-2}$ .

We first attempted to fit the available spectra with a 2-T MEKAL model with the global abundance of metals in the emitting plasma, relative to the solar value, left as a free parameter

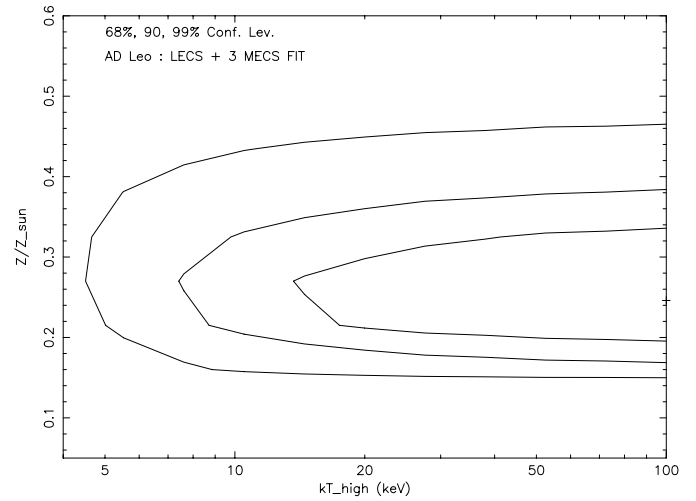


**Fig. 8.** The 68%, 90% and 99% confidence contours in the metallicity, high-T plane for the SAX spectra of AD Leo. This plot shows that while the value of the metallicity is well constrained by the SAX spectra, and the existence of an high temperature component is required to best fit the data, its value cannot be constrained.

in the fit, i.e. we have assumed that the abundances of individual elements have the same ratios as in the solar case. The resulting best-fit model is shown in Fig. 6, together with the observed spectrum. This fit yields a value of  $\chi^2$  of 185.1 with 145  $\nu$  corresponding to a null-hypothesis probability of 1.4% to give an adequate description of the AD Leo coronal spectrum. In other words the adopted model does not give an acceptable description of available data. The analysis of the uncertainties of the best-fit parameters yields the 90% confidence intervals summarized in Table 5, together with the best-fit parameters. The confidence intervals show that we can only set a lower-limit to the value of the high-temperature. In order to obtain an acceptable fit we have added a third thermal MEKAL component and have repeated the fit leaving the metallicity free to vary. The resulting best-fit model is shown in Fig. 7. The fit formally converges with a value of  $\chi^2$  of 163.0 for 145  $\nu$  corresponding to a probability level of  $\sim 9.0\%$ , but with the hotter component having a “best-fit” value of temperature extremely high (and unrealistic) and essentially unconstrained, as it is shown by the  $\chi^2$  contours in Fig. 8. In summary, the available data constrain the value of metallicity to be lower than solar, and they require the presence of a hot component whose temperature can only be stated to be higher than  $\log(T) = 8.13$ . Available data do not allow us to discriminate between the (assumed) thermal and a non-thermal nature of this hot component.

### 3.2.2. The SAX spectra of EV Lac

Given the small source distance and the fits of PSPC spectra we have decided to adopt  $N_H = 10^{19} \text{ cm}^{-2}$ . We have checked that no acceptable fit can be obtained with a lower hydrogen column density.

We first attempted to fit the available spectra with a 2-T MEKAL model with metallicity left free to vary. This fit yields a

**Table 5.** Summary of best multi-temperature fits of SAX spectra

Star	Z ( $Z/Z_{\odot}$ )	$\log(T_1)$ (K)	$EM_1$ ( $10^{51} \text{ cm}^{-3}$ )	$\log(T_2)$ (K)	$EM_2$ ( $10^{51} \text{ cm}^{-3}$ )	$\log(T_3)$ (K)	$EM_3$ ( $10^{51} \text{ cm}^{-3}$ )	Prob (%)	$f_X$ ( $10^{-11} \text{ erg/s/cm}^2$ ) [0.1–7.0 keV]
AD Leo									
2T	0.14 [0.13–0.15]	6.95 [6.93–6.97]	4.5 [4.2–4.9]	8.27 [>6.43]	0.28 [0.26–0.38]	...	...	1.4	1.38
3T	0.25 [0.22–0.35]	6.57 [6.48–6.69]	1.5 [1.2–1.8]	7.06 [7.02–7.09]	2.6 [2.2–3.2]	9.06 [>8.13]	0.27 [0.21–0.31]	9.0	1.40
EV Lac									
2T	0.27 [0.20–0.40]	6.84 [6.75–6.89]	1.2 [0.8–1.5]	7.40 [7.35–7.48]	0.8 [0.7–1.2]	...	...	1.0	1.07
3T	0.59 [0.36–1.11]	6.50 [6.39–6.60]	0.45 [0.25–0.63]	6.92 [6.80–7.00]	0.38 [0.21–0.75]	7.40 [7.36–7.43]	0.77 [0.65–0.95]	2.9	1.12

1 The reported parameter uncertainty ranges are computed at 90% confidence level assuming a single interesting parameter.

2 All the AD Leo fits were performed assuming  $N_H = 10^{18} \text{ cm}^{-2}$ .

3 All the EV Lac fits were performed assuming  $N_H = 10^{19} \text{ cm}^{-2}$ .

value of  $\chi^2$  of 103.8 for 78  $\nu$  corresponding to a probability of 1% to give an adequate description of EV Lac coronal spectrum. Again the adopted model does not give a satisfactory description of the data (i.e. the probability is lower than the 3% limit we have adopted). In order to improve our model description we have added a third thermal MEKAL component and have repeated the fit leaving the metallicity free to vary. The fit yields a value of  $\chi^2$  of 95.2 (for 78 degree of freedom) that corresponds to a null hypothesis probability of 2.9%, i.e. a marginally acceptable fit. The limited statistic of the available spectra does not allow us to attempt a fit with a more complex model. The resulting best-fit parameters for these two models are summarized in Table 5, together with the 90% confidence error intervals. We note that the EV Lac results are qualitatively similar to those for AD Leo.

#### 4. Loop modeling and discussion

The analysis of the AD Leo spectra shows that its coronal spectrum has a complex thermal structure, as revealed by the different value of temperatures obtained by fitting data from different instruments. In very general terms the emission peaks around  $\log T \approx 6.8$ –6.9, as demonstrated by the best-fit emission measure values derived with the PSPC and with SAX. The existence of emission from hotter plasma suggested by the PSPC spectral fit, is confirmed by the analysis of the SAX spectra. All the spectral fitting results point toward a coronal metallicity below solar. However it is worth to note that the derived value of coronal metallicity depends significantly (up to a factor 2) from the model adopted to describe the complex thermal structure of the observed spectra. This result points out one of the inherent difficulties in obtaining trustful determination of coronal metallicity (and even more of coronal abundances) based on low or medium resolution X-ray spectra.

The analysis of the EV Lac spectrum shows a similar complexity of the thermal structure, with most of the coronal plasma at temperature around or above  $\log T=6.8$ . During the strong

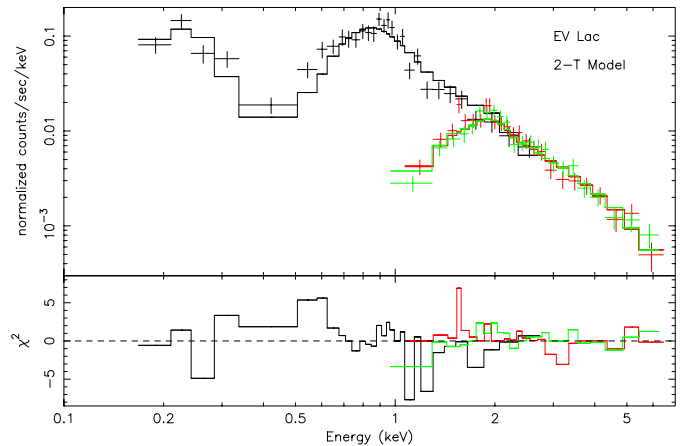


**Fig. 9.** The observed SAX spectra of EV Lac together with the best-fit two-temperature MEKAL spectrum, yielding a global metallicity 0.27 times solar. The bottom panel y-axis shows the (signed) contribution of each bin to the total  $\chi^2$ .

flare seen in one of the PSPC observation an additional thermal component with temperature around  $\log T=7.6$  (and certainly above  $\log T=7.27$ ) appears. While the PSPC spectra indicate a coronal metallicity below solar, this is not confirmed by the analysis of higher resolution and wider bandpass SAX spectra that are instead compatible with coronal metallicity being solar or only marginally sub-solar. Even a 3-T plasma model does not give a completely satisfactory fit to the SAX spectra, since the resulting probability is just below our acceptance threshold of 3%.

In view of the complexity of the thermal structure of the coronae of AD Leo and EV Lac, we have attempted to fit the SAX spectra with a model synthesized from constant cross-section static coronal loops (Serio et al. 1981, Ciaravella et al. 1996). This modeling approach has been recently adopted to fit the PSPC spectra of F and G-type stars (Maggio & Peres 1997,

**Table 6.** Summary of 2-loop model fits of SAX Spectra

Star	Z ( $Z/Z_{\odot}$ )	Log( $T_{max1}$ ) (K)	Log( $l_1/R_*$ )	$f_1$	Log( $T_{max2}$ ) (K)	Log( $l_2/R_*$ )	$f_2$	Prob (%)
AD Leo	0.23 [0.20–0.30]	7.12 [7.09–7.14]	−2.3 [< −1.0]	1.6e−4 [<3.1e−3]	8.5 [> 8.2]	−2.1 [unconstrained]	1.0e−10 [unconstrained]	7.3
EV Lac	0.45 [0.32–0.69]	6.90 [6.74–7.01]	−2.3 [< −1.4]	2.1e−4 [<1.7e−4]	7.53 [7.47–7.58]	−2.3 [< −1.2]	9.4e−7 [<1.2e−5]	1.7

1 The reported parameter uncertainty ranges are computed at 90% confidence level assuming a single interesting parameter.

2 All the AD Leo fits were performed assuming  $N_H = 10^{18} \text{ cm}^{-2}$ .

3 All the EV Lac fits were performed assuming  $N_H = 10^{19} \text{ cm}^{-2}$ .

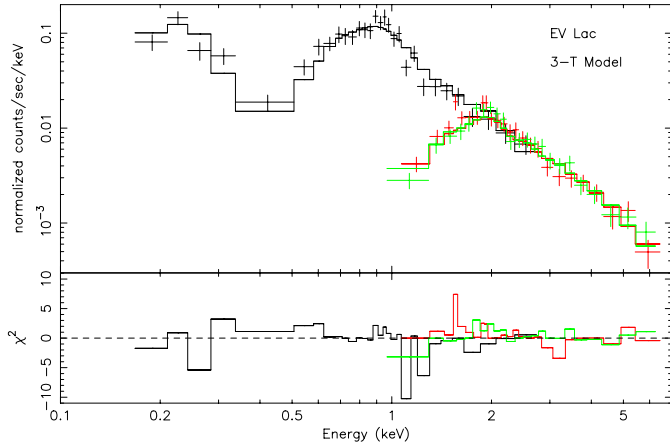


**Fig. 10.** The observed SAX spectra of EV Lac together with the best-fit three-temperature MEKAL spectrum, yielding a global metallicity 0.59 times solar. Again note that most of improvement in the fit occurs in the spectral region around 0.6 keV. The bottom panel y-axis shows the (signed) contribution of each bin to the total  $\chi^2$ .

Ventura et al. 1998). The reliability of the adoption of static loop models to describe physical conditions that are clearly dynamic, such as the flares occurring both on AD Leo and EV Lac, has been extensively discussed by Reale & Micela (1998) and by Ventura et al. (1998). In summary, if the flaring events occurs – as it is usually the case – on timescales much shorter than the hydrodynamic one, then the time scale of the evolution of the plasma inside the loop is much longer than that of the heating and the latter acts as if it were constant. Under such a condition, the experience with solar case suggests that the emission spectrum approaches the one emitted from a loop in stationary conditions.

As an extension to the works cited above, in order to take into account the evidence that, at least in the case of AD Leo, the value of the coronal metallicity is sub-solar, we have constructed a grid of coronal loop models having as free parameter also the plasma metallicity, beside the loop length,  $l$ , and the plasma maximum temperature,  $T_{max}$ . This model has as further free parameter in the fit the surface filling factor,  $f$ , i.e. the fraction of stellar surface covered by a given class of loops. This grid of models has been arranged to be used as one of the external tabular models of XSPEC V10.0. Model calculation at various coronal metallicities has been performed in a self-consistent

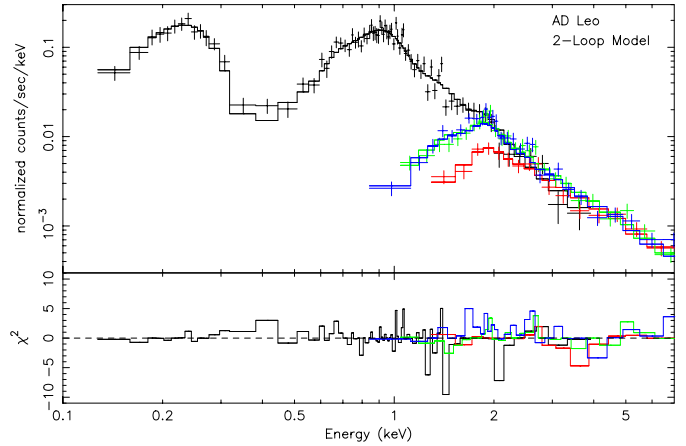


**Fig. 11.** The fit of the SAX spectra of AD Leo with a model of emission from a 2 coronal loop plasma model. For this fit the hydrogen column density has been taken fixed to  $\log N_H = 18$ . The bottom panel y-axis shows the (signed) contribution of each bin to the total  $\chi^2$ .

tent way, using the MEKAL emissivity and integrating along the loop the contributions from the continuous emission measure distribution and considering the effect of coronal metallicity on the radiative loss function, i.e. on the final loop thermal structure.

Armed with this specific tool we fitted the collected spectra and we have found that no single loop model can give an adequate description of the observed spectra. We have then added a second loop component to our model obtaining the fitting results shown in Figs. 11 and 12 for AD Leo and EV Lac, respectively. As a matter of fact the “quality” of the best-fit 2-loop models, as measured by the probability level of the  $\chi^2$  test, is (see Tables 5 and 6) better than for the 2-T models, and slightly worse than for the best-fit 3-T models. Note that 3-T models and loop models have the same number of fitted parameters. A summary of the best-fit loop modeling is given in Table 6.

In order to properly interpret the above findings it is necessary to recall that if the loop length is smaller than the pressure scale height,  $H = 2kT_{max}/\mu g = 6000T_{max}/(g/g_{\odot})$  (where  $g$  is the stellar gravity, and  $T_{max}$  is in units of K) the solution of the loop static equations imply the so-called RTV (Rosner et al. 1978) scaling law among  $T$ ,  $l$  and the loop base pressure,  $p$ , namely  $T_{max} = 1.4 \cdot 10^3 (pl)^{1/3}$ , a result clearly confirmed

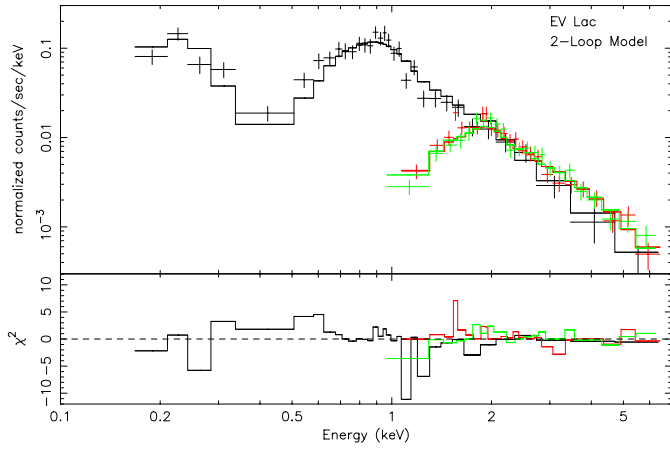


**Fig. 12.** The fit of the SAX spectra of EV Lac with a model of emission from a 2 coronal loop plasma model. Note that, similarly, to the 3-T fit case, the fit is statistically unsatisfactory mostly because the model does not reproduce the emission below 0.5 keV. For this fit the hydrogen column density has been taken fixed to  $\log N_H = 19$ , however leaving free to vary the value of  $N_H$  improves only marginally the fit. The bottom panel y-axis shows the (signed) contribution of each bin to the total  $\chi^2$ .

by the solar observations. We want to stress that, because of this scaling law, any fitting procedure cannot determine separately  $p$  and  $l$  at the same time. This result is due to the scaling invariance of the equations describing the problem (see Maggio & Peres 1996), and it is responsible for the elongated shape of  $\chi^2$  confidence regions in any  $p$ - $l$  plane (cf. Serio 1996).

Our fit results are consistent with loops having lengths much smaller than the pressure scale height, hence RTV scaling law applies. In this case,  $T_{max}$  (and hence the product  $pl$ ) is the only parameter well constrained by the fit, while the other quantities, including the surface filling factor, may take a range of possible values while yielding the same quality of the fitting result. We reiterate that this is an *intrinsic* property of the model and *cannot* be overcome. However, the statistical confidence regions in the model parameter space allow us to derive an upper limit on the length (and hence a lower limit on the loop base pressure), and an upper limit also on the related area coverage fraction, in practice lower than the obvious constraint  $f < 1$ . This is true for all loop components, with the exception of the high- $T_{max}$  loop required to fit the high energy tail of the AD Leo spectrum, because  $l_2/R_*$  is unconstrained. It is worth to stress that loops with  $l/R_*$  even smaller than our best-fit solution can give, formally, an adequate description of the emitted spectrum.

Moreover, note that the overall X-ray luminosity emitted by a given loop can be expressed as

$$L_X \sim 2.16 \cdot 10^{16} \gamma (R_*/R_\odot)^2 T_{max}^{7/2} f l^{-1} \text{ erg/sec} \quad (1)$$

$$= 5.9 \cdot 10^{25} \gamma (R_*/R_\odot)^2 T_{max}^{1/2} f p \text{ erg/sec}, \quad (2)$$

where  $\gamma$  is the fraction of energy input (heating) that is emitted in the X-ray band (see G96). Since  $T_{max}$  is usually well determined, the overall observed luminosity constrains the

quantity  $f/l$  (or  $fp$ ); this is the way in which we have estimated the upper limits on  $f$  from the upper limits on  $l$ , as reported in Table 6.

In summary, for a given maximum temperature, the observed X-ray luminosity depends only on the product  $fp$  (or  $f/l$ ). Since  $T_{max}$  and  $lp$  are related by the scaling laws, the above dependence implies that, for loop lengths shorter than the pressure scale height,  $l$ ,  $p$  and  $f$  can occupy a range of admissible solutions (possibly limited also by the constraint  $f < 1$ ). In other words, when  $l < H$ , the loop modeling cannot provide *one solution*, but instead a range of admissible solutions with different area coverage and base pressure (or length) of the emitting loop. In any case, the above fitting results with loop models allow us to infer some of the properties of the stellar coronae, which could not be otherwise derived (and certainly not with multi-component isothermal models, lacking sufficient physical basis).

As a further step in the interpretation of the fitting results, let us consider that the area coverage factor can be written as

$$f = N\alpha^2\beta^2/4, \quad (3)$$

where  $N$  is the number of loops of a given component,  $\alpha$  is the loop aspect ratio, i.e. the ratio between loop base radius and length<sup>3</sup>,  $\beta = l/R_*$  is the ratio between loop length and stellar radius. For each of the loop components we have derived the values of  $f$  and of  $\beta$ , hence we can deduce the value of  $N$  as a function of the loop aspect ratio. Recall that  $f/\beta$  is constant within the confidence regions determined by the fitting, as explained above.

Let us focus on the AD Leo low- $T_{max}$  loop: in this case our analysis gives a best-fit solution  $N\alpha^2 = 4f/\beta^2 \sim 25.5$ , and a formal 90% confidence limit which translates in  $N\alpha^2 > 1.24$ . Hence, for  $\alpha \sim 10^{-1}$  we would have a best-fit solution  $N \sim 2500$ , with a formal 90% confidence limit  $N > 124$ . Assuming instead the maximum loop aspect ratio,  $\alpha = 1/\pi$ , we would obtain  $N > 12$ . We interpret this findings as evidence that the lower  $T_{max}$  loops are indeed quite compact with length smaller than 0.1 stellar radius (and smaller than the pressure scale height) and that they cover a fraction not greater than 0.3% of stellar surface with tens to hundreds of loops.

Going to the high- $T_{max}$  loops, we have  $N\alpha^2 = 6.3 \cdot 10^{-6}$ , with the condition  $N \geq 1$ , this implies  $\alpha \leq 2.5 \cdot 10^{-3}$ , i.e. the solution is compatible with elongated and thin loops covering a very small fraction of the stellar surface. While we cannot set a 90% confidence limit on  $\beta$ , hence on the value of  $\alpha$ , yet if we assume as possible solution loops with  $\alpha \sim 0.1$ , i.e. typical solar loops, we can deduce<sup>4</sup> that the loop length should be extremely small,  $\leq 10^{-5}R_*$ , in order to meet the condition  $N > 1$ .

Similar arguments can be applied to the case of EV Lac: the 90% confidence limit on the length of the low- $T_{max}$  loops, together with the condition  $N \geq 1$ , would result in a formal

<sup>3</sup> For the given loop geometry, we have the constraint  $\alpha < 1/\pi \sim 0.32$  to avoid overlap of the loop foot-points

<sup>4</sup> We can compute  $\beta = 4/N\alpha^2 f/\beta$ , where  $f/\beta$ , being a constant, can be derived from the best fit values.

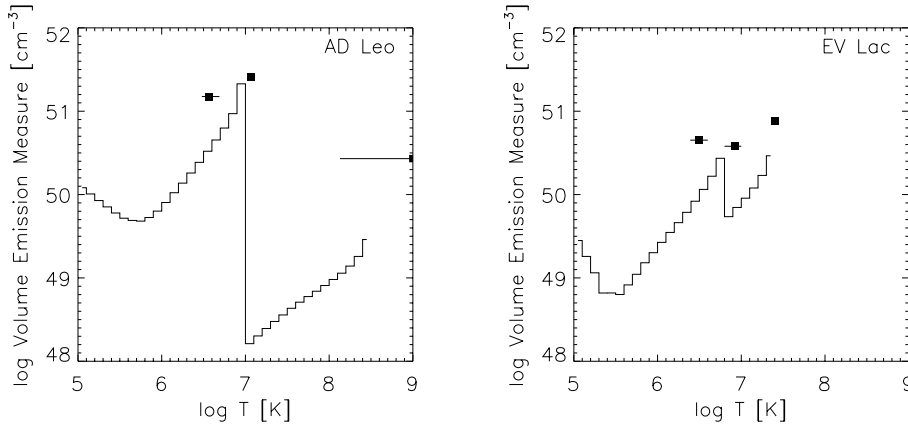


**Fig. 13.** The volume emission measure of AD Leo *left* and EV Lac *right* as derived from the two loop models that give the best-fits to the SAX spectra. The solid squares indicate the results of the three temperature fits, error bars on temperature are at the 90% confidence level.

aspect ratio  $\alpha < 0.66$ . Assuming the maximum allowed aspect ratio ( $\alpha = 0.32$ ), the above 90% confidence limit would result in  $N > 4$ . Adopting the same maximum aspect ratio to the best-fit solution would result in  $N > 327$ ; in the case of the high- $T_{max}$  loops, the 90% limit will result in  $\alpha < 0.11$ , and in a best-fit solution with  $N > 13$  for loops of this latter aspect ratio.

Our findings indicate that the coronae of active dM stars can be described by (at least) two major emitting structures (let say two major loop classes) with well distinct maximum temperatures. The corona of AD Leo is globally “hotter” than the corona of EV Lac. In both stars the loops with the lower  $T_{max}$  are compact (aspect ratio  $< 0.3$ -1.5), with length smaller than 0.1 stellar radius, base pressure higher than typical solar loops, and area filling factor of  $10^{-4}$ - $10^{-3}$ . There should be, at least, tens-hundreds of such loops to explain the observed emission. The higher  $T_{max}$  loops tend to have a more elongated structure (aspect ratio in the  $10^{-1}$ - $10^{-3}$  range), while maintaining a length smaller than 0.1 stellar radius. Because their area coverage factor is quite small, only at most ten of them are contemporary present in the corona. Given their elongated structure we argue that their base pressure is even higher than the pressure of the lower  $T_{max}$  loops, and they are likely to be non-steady and continuously replenished in the corona.

This picture is consistent with that derived from the analysis of AD Leo PSPC data (Giampapa et al. 1996), with our findings indicating that the high  $T_{max}$  component being due to very high pressure, elongated loops covering a very small fraction of stellar surface, i.e. we rule out, between the two possible interpretations proposed by G96, the one implying the presence of loops having length comparable to the stellar radius.

In the case of EV Lac both the 2-loop fit, and the 3-T one, are statistically inadequate, hence our interpretation should be taken with some caution. It is worth to notice that these fits are unsatisfactory (at the adopted 3% probability acceptance threshold) mostly because the models are inadequate to predict the emitted spectrum below 0.5 keV. This cannot be improved even allowing the hydrogen column density to reach an unrealistically high value.

While we have not done detailed analysis of any specific flare, yet our results seem to contradict the existence of AD Leo loops with length comparable to the stellar radius (Cully

et al. 1997), while it is more consistent with the recent analysis of the AD Leo flare seen with the ROSAT PSPC that has been interpreted as occurring on a loop whose length was of the order of 0.1 stellar radius (Reale & Micela 1998).

Apart from a change in the absolute flux level, which however is within the range common in active coronal sources, the SAX observation of AD Leo and EV Lac are in agreement with the IPC, and/or the PSPC ones.

To go further in our analysis we show in Fig. 13 the resulting volume emission measure (VEM) distribution for the best-fit two loop model we have derived for AD Leo. This VEM is distinctly different from that derived from the analysis of PSPC data of nearby dG stars (Ventura et al. 1998) with substantial emitting plasma above  $\log T=7.0$ , and the lower  $T_{max}$  being higher than the equivalent value in the case of dG stars. Moreover it is interesting to note that the best-fit 3-T model yields  $\log T_1 = 6.55$ ,  $\log T_2 = 7.04$ , and  $\log T_3 = 8.96$ . The latter two match the VEM peak (at  $\log T \sim 7$ ) and the VEM high temperature tail ( $\log T \leq 8.5$ ), while the low temperature component is needed to describe the contribution of plasma with  $\log T$  below and around 6.0. While the above analysis makes it clear the “relation” between the best-fit 3-T and loop models, it is also evident that only this latter model allows us to gain a deeper physical insight on the nature of the emitting coronal structures, that cannot be derived from the adoption of the multi-thermal emitting models.

Finally, in the light of the controversy about the presence of significant differences between photospheric and coronal abundances in active stars it is worth to investigate if the coronal and photospheric abundances of AD Leo are compatible with each other. The most recent photospheric abundance analysis (Jones et al. 1996) of AD Leo based on high resolution IR spectra around the 1.2 micron region results in a best-fit solution with  $T_{eff} = 3350 \pm 50$  K,  $[Z/H] = -0.75 \pm 0.25$ , and  $\log g = 4.5 \pm 0.25$ , to be compared with the expected stellar parameters  $T_{eff} = 3230 \pm 150$  K,  $[Z/H] = 0.0 \pm 0.5$ , and  $\log g = 4.73 \pm 0.15$ . A different determination of  $[Z/H]$  has resulted in the value  $0.4 \pm 0.3$  (Naftilan et al. 1992).

We interpret the above results as an indication that, at the moment, no clear cut answer can be given on the photospheric metallicity of AD Leo hence it could be possible that its coronal

metallicity, as derived from the SAX spectra, is indeed compatible with its intrinsic photospheric metallicity.

In conclusion, the SAX X-ray spectra of AD Leo does not appear to support the classification of this star among the so-called Metal Abundance Deficiency syndrome stars (see Drake 1996 for a review about this issue).

*Acknowledgements.* SS, and AM acknowledge partial support from ASI and MURST. We would like to thank A. N. Parmar, R. Pallavicini, G. Micela and G. Peres for the many enlightening discussions.

## References

- Avni Y., 1976, *ApJ* 210, 642
- Barbera M., Micela S., Sciortino S., Harnden, F.R.J., Rosner R., 1993, *ApJ* 414, 846
- Boella G., Butler R.C., Perola G.C., et al., 1997a, *A&AS* 122, 299
- Boella G., Chiappetti L., Conti G., et al., 1997b, *A&AS* 122, 327
- Ciaravella A., Peres G., Maggio A., Serio S., 1996, *A&A* 306, 553
- Cully S., Fisher G., Hawley S.L., Simon T., 1997, *ApJ* 491, 910
- Delfosse X., Forveille T., Perrier C., Mayor M., 1998, *A&A* 331, 581
- Drake J.U., 1996, In: Pallavicini R., Dupree A. (eds.) *Cool Stars, Stellar Systems, and the Sun. Ninth Cambridge Workshop, ASP Conf. Series Vol. 109, ASP*, 203
- Durney B.R., De Young D., Roxeburg I.W., 1993, *Solar Phys.* 145, 207
- Eggen O.J., 1973, *PASP* 85, 542
- Favata F., 1998, In: Donahue R.A., Bookbinder J.A. (eds.) *Cool Stars, Stellar Systems, and the Sun. 10th Cambridge Workshop, Vol. in press*
- Favata F., Maggio A., Peres G., Sciortino S., 1997, *A&A* 326, 101
- Favata F., Maggio A., Peres G., Sciortino S., 1998, In: Donahue R.A., Bookbinder J.A. (eds.) *Proceedings of the 10-th Cambridge Workshop on Cool Stars. PASB, in press*
- Giampapa M.S., Rosner R., Kashyap V., Fleming T.A., Schmitt J.H.M.M., 1996, *ApJ* 463, 707
- Jones H.R.A., Longmore A.J., Allard F., Hauschildt P.H., 1996, *MNRAS* 280, 77
- Lampton M., Margon B., Bowyer S., 1976, *ApJ* 208, 177
- Maggio A., Peres G., 1996, *A&A* 306, 563
- Maggio A., Peres G., 1997, *A&A* 325, 237
- Maggio A., Sciortino S., Harnden F.R.J., 1994, *ApJ* 432, 701
- Meyer J.-P., 1985, *ApJS* 57, 173
- Micela G., Pye J., Sciortino S., 1997, *A&A* 320, 865
- Naftilan S.A., Sandmann W.S., Pettersen B.R., 1992, *PASP*, 104
- Pallavicini R., 1998, In: Scarsi L., Bradt H., Giommi P., Fiore F. (eds.) *The Active X-ray Sky: Results from BeppoSAX and Rossi-XTE. Nuclear Physics B (Proc. Suppl.)* 69, 56
- Pallavicini R., Monsignori-Fossi B., Landini M., et al., 1988, *A&AS* 191, 109
- Parmar A.N., Martin D.D.E., Bavdaz M., et al., 1997, *A&AS* 122, 1
- Preibisch T., 1997, *A&A* 320, 525
- Raymond J., 1988, In: Pallavicini R. (ed.) *Hot thin plasmas in Astrophysics. Kluwer, Dordrecht*, 3
- Raymond J., Smith B., 1977, *ApJS* 35, 419
- Reale F., Micela G., 1998, *A&A* 334, 1028
- Rosner R., Tucker W.H., Vaiana G.S., 1978, *ApJ* 220, 643
- Saar S.H. 1990, In: Stenflo J.O. (ed.) *Solar Photosphere: Structure, Convection and Magnetic Fields. Kluwer, Dordrecht*, 427
- Schmitt J.H.M.M., Collura A., Sciortino S., et al., 1990, *ApJ* 365, 704
- Schmitt J.H.M.M., Fleming T.A., Giampapa M.S., 1995, *ApJ* 450, 392
- Serio S., 1996, In: Uchida Y., Kosugi T., Hudson H. (eds.) *Magnetodynamic Phenomena in the Solar Atmosphere - Prototypes of Stellar Magnetic Activity. Kluwer, Dordrecht*, 63
- Serio S., Peres G., Vaiana G.S., Golub L., Rosner R., 1981, *ApJ* 243, 288
- Stern R., Schmitt J., Kahabka P., 1995, *ApJ* 448, 683
- Vaiana G.S. 1983, In: Stenflo J.O. (ed.) *Solar and Stellar Magnetic Fields: Origins and Coronal Effects. Reidel, Dordrecht*, 165
- Ventura R., Maggio A., Peres G., 1998, *A&A* in press
- White N.E. 1996, In: Pallavicini R., Dupree A. (eds.), *Cool Stars, Stellar Systems, and the Sun. Ninth Cambridge Workshop, ASP Conf. Series Vol. 109, ASP*, 193